SUPPORTING INFORMATION

Single Molecule Trapping and Sensing using Dual Nanopores separated by a Zeptolitre Nanobridge

Paolo Cadinu[1,2], Binoy Paulose Nadappuram[1], Dominic J. Lee[1], Jasmine Y.Y Sze[1], Giulia Campolo[1], Yanjun Zhang[3], Andrew Shevchuk[3], Sylvain Ladame[2], Tim Albrecht[1], Yuri Korchev[3], Aleksandar P. Ivanov[1,*], Joshua B. Edel[1,*]

[1] Department of Chemistry, Imperial College London, SW7 2AZ, United Kingdom
[2] Department of Bioengineering, Imperial College London, SW7 2AZ, United Kingdom
[3] Department of Medicine, Imperial College London, W12 0NN, United Kingdom

*E-mail correspondence: joshua.edel@imperial.ac.uk, alex.ivanov@imperial.ac.uk
phone number: 020 7594 0754

Table of Contents

Experimental details

Nanopipette fabrication

Nanopipettes were fabricated using a P-2000 laser puller (Sutter Instrument Co) from quartz theta capillaries (QF120-90-7.5; Sutter Instrument Co) with an outer diameter of 1.2 mm. The inner diameter, which measured 0.9 mm, is divided into two chambers insulated by a septum of thickness 0.15 mm. The latter retains its shape also after the capillary has been laser-pulled. Nanopipettes were fabricated using the following protocol: (1) HEAT, 850; FIL, 4; VEL, 30; DEL, 160; PUL, 80, followed by (2) HEAT, 860; FIL, 3; VEL, 20; DEL, 140; PUL, 160. It should be noted that the above parameters are instrument specific and might have slight variations due to local temperature and humidity. Silanization process consisted in exposing for 5 seconds the back end of the nanopipette to Trichloro(1*H*,1*H*,2*H*,2*H*-perfluorooctyl)silane (# 448931-10G) purchased from Sigma.

Single channel recording

The ionic current was measured by applying a voltage bias across a pair of Ag/AgCl electrodes (0.125 mm diameter, GoodFellow U.K.). Depending on the configuration the electrodes were placed differently: Nanobridge and bulk configuration, one electrode in each barrel of the nanopipette, conventional, one electrode was placed in one barrel of the nanopipette while the other electrode was placed in the bath. The current was measured with an Axopatch 200B low noise current amplifier (Molecular Devices) in "voltage clamp" mode. Data were low-pass filtered using a built-in Bessel filter. The analog signal was digitized at 100 kHz using Digidata 1440A data-acquisition module (Molecular Devices). Data analysis was carried out using a custom written Matlab analysis routine. 10 kbp, 5 kbp dsDNA ($500mg\ ml^{-1}$) , the 1 kbp dsDNA ladder and the ssRNA ladder ($2000mg\ ml^{-1}$) were purchased from New England Biolabs. 1.5 kbp, 500 bp, 200 bp NoLimits™ individual DNA fragments with a stock concentration of $500mg\ ml^{-1}$ were purchased from Thermo Scientific. All DNA solutions / dilutions were prepared in 100 mM KCl, 10 mM Tris, 1 mM EDTA at pH 8.0.

ssDNA preparation

Linearization of m13mp18. Single stranded circular DNA m13mp18 7.2 kb was purchased from (NEB Hitchin, UK). A linear scaffold was required in order to perform translocation experiment. The linear version was made by hybridising a 22 and 23 base oligonucleotide to allow the cutting of SpHI and SnaBI (NEB Hitchin, UK) restriction site respectively. Circular M13 was mixed with 10x molar excess of each oligonucleotide at 90°C and annealed at 65°C in a buffer containing 10 mM Tris-HCL, 1 mM EDTA and 5 mM $MgCl_2$ at pH 8.0 before cooling to 25°C. 1 ml of SphI and 2 ml of SnaBI (10,000 units/mL) and (5,000 units/ mL) respectively were then added to the DNA mixture and incubate overnight at 37°C. The linearized M13 were purified using a QIAquick miniprep kit (Qiagen, CA USA) and the enzymes and excess unbound nucleotides were removed by PCR clean-up gel extraction (Macherey-Nagel, Germany).

DNA labelling and imaging

Fluorescently labelled DNA samples for imaging was prepared by incubating 250 pM 10 kbp DNA solution in 10 mM Tris 1 mM EDTA with YOYO-1 (Molecular Probes) at a ratio of five base pairs per YOYO-1 molecule. The nanopipette was filled with the labelled DNA solution and mounted onto a single axis micromanipulator (Thor Labs, USA) which in turn was mounted onto a microscope stage. Images and videos were acquired by using a 60X water-immersion objective (1.20 NA,

UPLSAPO 60XW, UIS2, Olympus) in conjunction with an electron multiplying CCD (emCCD) camera (Andor, iXon Ultra-887). The fluorescently labelled DNA sample inside the pipette was excited using a 488 nm continuous-wave solid-state laser (Sapphire 488LP, Coherent). The emCCD camera consists of a 512x512 frame size with each pixel being 16 μm, this corresponds to an imaging resolution of 267 nm with a 60x objective. For the optical measurements translocations were performed using a patch-clamp amplifier (A-M systems 2400, USA).

Nanobridge size characterization

The size of the nanobridge formed at the pipette tip was estimated by using SECCM type approach curve measurements[48]. For this, both barrels of the nanopipette were filled with 100 mM KCl solution (buffered with 10 mM Tris 1 mM EDTA, pH 8.0) to form droplet nanobridge at the tip of the nanopipette. Ag/AgCl electrodes were then inserted into each of the barrel to establish electrical contact. The nanopipette was mounted onto a single axis (z) piezoelectric positioner (P-753-3CD, Physik Instrumente) perpendicular to a quartz substrate to control the position of the nanopipette during the approach. The quartz substrate surface was silanized to minimize droplet adsorption to the quartz surface. A 400 mV bias was applied between the Ag/AgCl electrodes to induce an ion current (I_{DC}) between the barrels, across the droplet. This I_{DC} was measured and recorded by using MultiClamp 700B amplifier (Molecular Devices) with a digitizer (Digidata® 1550, Molecular Devices). The magnitude of I_{DC} was used as a feedback signal to detect contact between the droplet meniscus and the surface and to control the separation between the tip of the nanopipette and the surface. A 30 to 60 % decrease in I_{DC} was used as the feedback to detect tip-surface contact. Upon tip-surface contact, the ionic current decreases to a minimum value, but increases afterwards when the nanopipette crashes into the glass substrate, breaking the tip and thereby increasing its diameter. A 60% change in I_{DC} was used as the feedback to halt the approach after it crashes into the glass substrate. The height difference (Δz) recoded between the initial droplet contact with the surface and the tip-surface contact corresponds to the size of the nanobridge formed at the tip of the nanopipette.

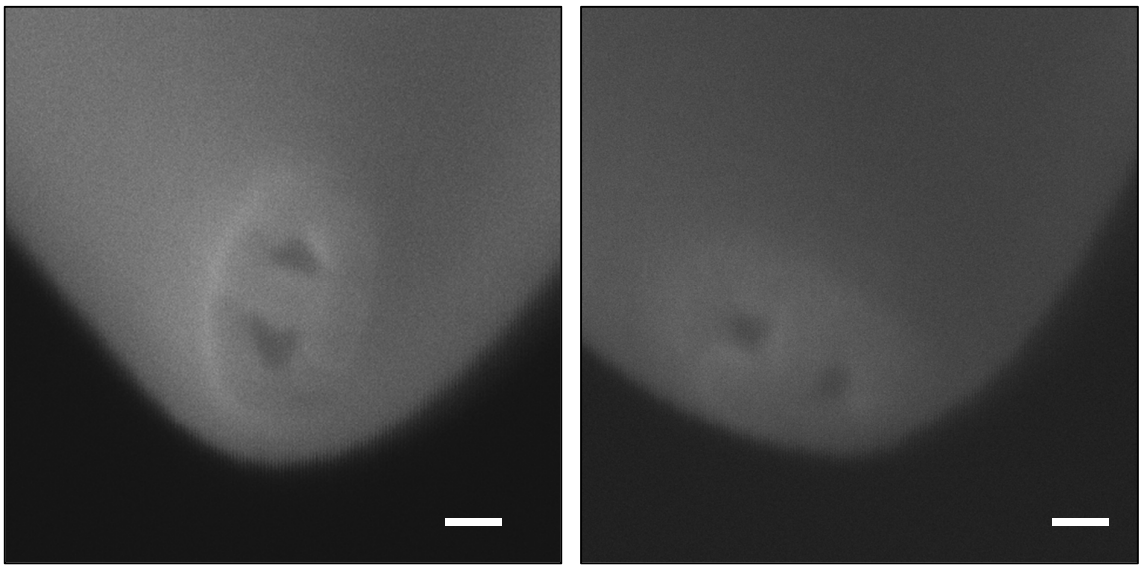

Figure S1. SEM images of representative dual barrel nanopipettes. Nanopippetes were fabricated by laser assisted pulling of quartz capillaries. Dual nanopores are visible at the nanopipette tips. Scale bars are 20 nm.

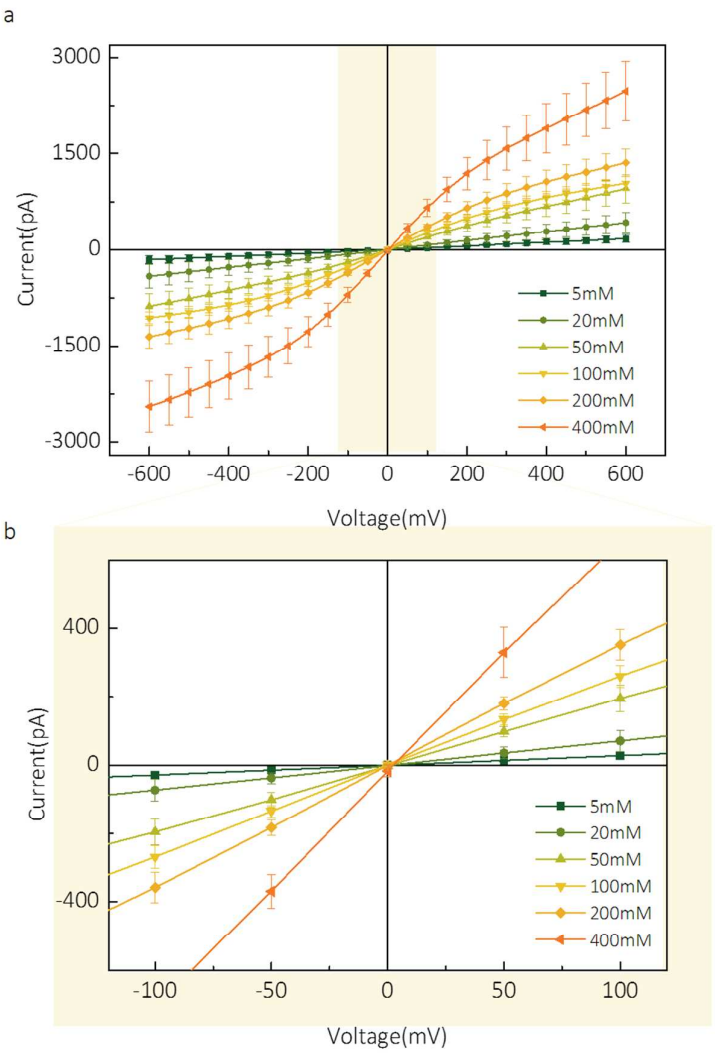

Figure S2. Salt concentration dependence of the nanobridge configuration. (a) Current voltage curves averaged over at least 3 nanopipettes at 0.005, 0.02, 0.05, 0.1, 0.2 and 0.4 M KCl 10 mM Tris 1 mM EDTA pH 8.0, respectively. All I-Vs exhibit quasi-sigmoidal characteristics which were more pronounced at higher ionic strength. Notably above 0.1 M KCl, the number of working devices decreases significantly in part due to the likelihood of salt crystallization within the nanobridge. (b) Zoomed in region at $\pm$100 mV, showing ohmic response.

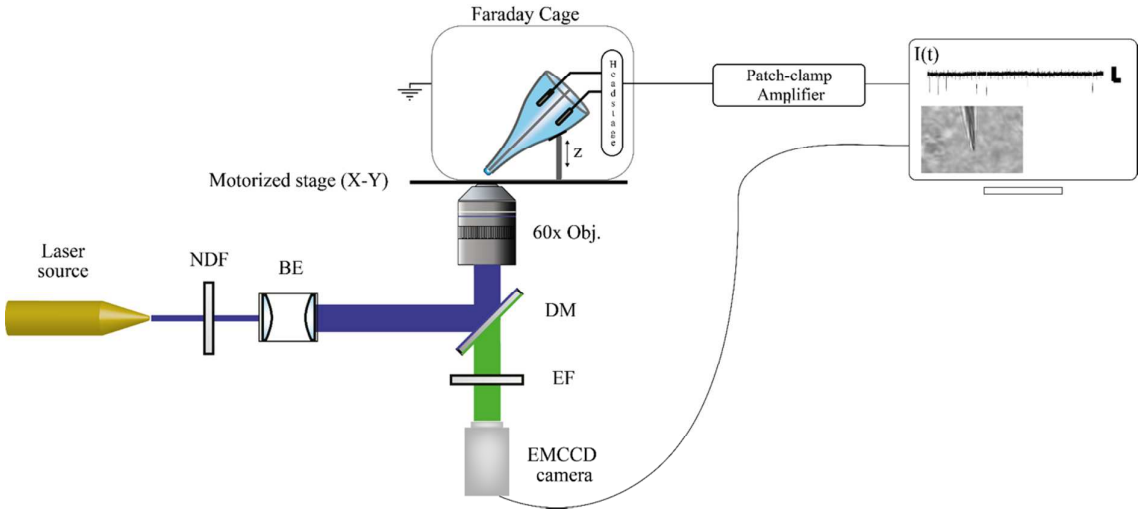

Figure S3. Schematic of the setup used for fluorescence imaging and characterization. Please see description below.

Fluorescence experiments were conducted on a custom-built microscope. Briefly, the excitation light was generated by using a continuous-wave solid-state laser (λ_{EX} = 488 nm, Sapphire 488LP, Coherent, USA) and was focused on to the sample via a long pass dichroic mirror (DM) through a 60x water immersion objective lens (UPLSAPO 60XW, Olympus, USA) having a Numerical Aperture (NA) of 1.2 and working distance (WD) of 0.28 mm. A beam expander (BE) was used to entirely fill the back aperture of the objective and the light was attenuated as needed using neutral density filters (NDF). The emitted light from the tip of the nanopipette was collected back through the same objective, transmitted through the DM and long pass emission filter and focussed on to an emCCD camera (iXon Ultra 897, Andor Technologies, UK). The fluorescence emitted by the sample was then focused onto emCCD camera detector by the same objective. A controller unit (ProScan II, Prior Scientific) was used to precisely control the motorized stage (H1117, Prior Scientific, USA) and the z-axis focus motor ensuring accurate sample position. A custom dichroic filter (Chroma Technology) was used to isolate the laser excitation source from the emitted fluorescence light. The dual barrel nanopipettes using in the nanobridge configuration was mounted on a single-axis miniature translational stage (DT12, ThorLabs, USA) and used to manually approach the nanopipette to within the WD of the objective. The translational stage was placed on top of a motorized stage (Prior Scientific US) consisting of a universal sample holder (H473XR, Prior Scientific USA). To perform translocation experiments, a pair of Ag/AgCl electrodes were inserted into each barrel and connected to the amplifier head stage of a patch clamp (A-M 2400, A-M Systems, USA) which was used to apply the potential. To shield electromagnetic radiation, the universal sample holder, onto which the nanopipette and the head stage were mounted, was enclosed in a Faraday cage. The analogue signal coming from the amplifier head stage signal was filtered by an integrated 4 pole Bessel low pass filter and then digitalized using a Data Acquisition Card (NI-USB 6259, National Instrument, USA). All traces were recorded with WinWCP Strathclyde Electrophysiology software freely distributed by University of Strathclyde Glasgow.

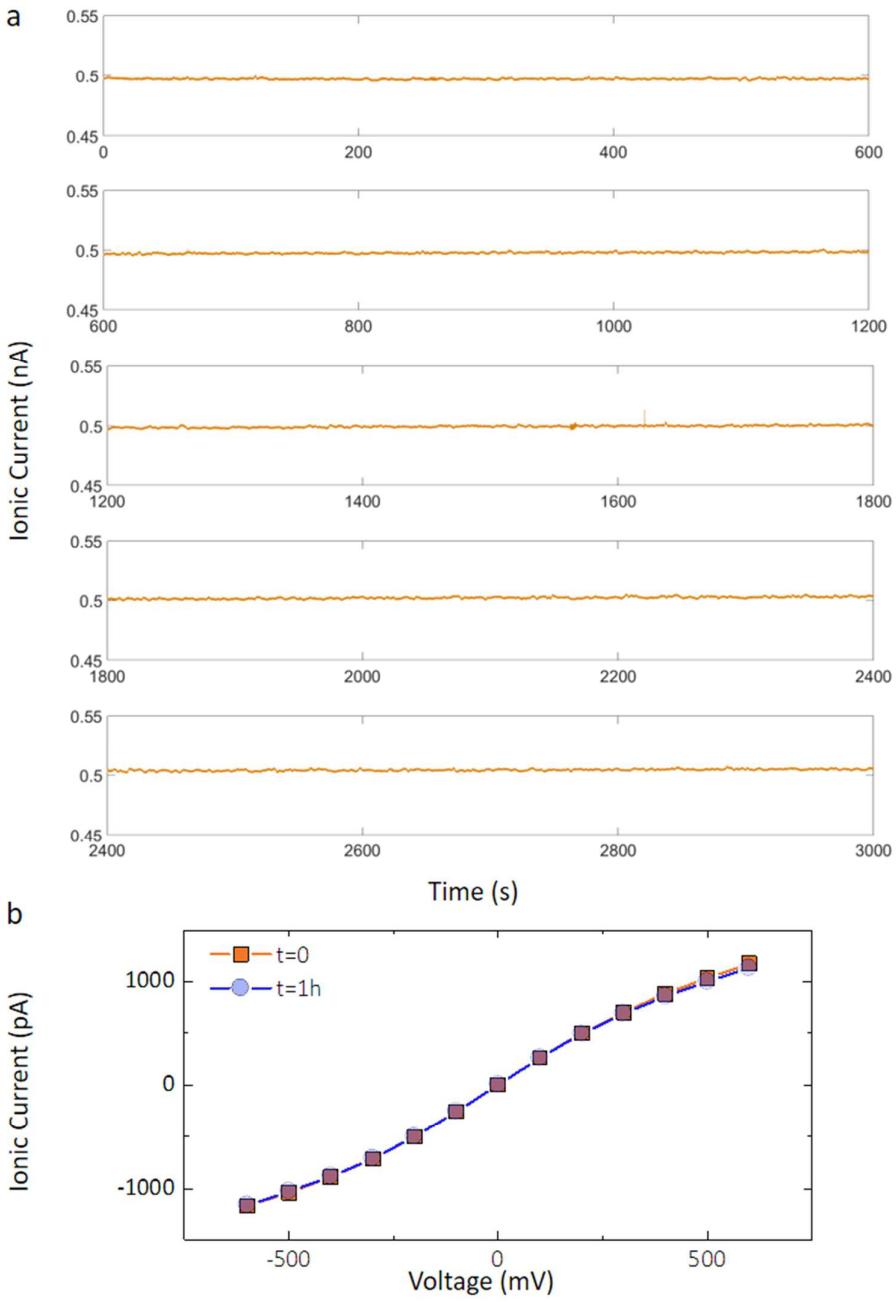

Figure S4. Characterization of droplet stability using the nanobridge configuration. (a) An ionic current time trace is shown using 100 mM KCl 10 mM Tris 1 mM EDTA (pH 8.0) and recorded at 200 mV applied bias. The trace has been resampled at 1 kHz for visualization purposes. Importantly the open pore current was exceptionally stable over long time periods. For example, at time t=0 the mean current was 497 ± 1 pA; after 50 minutes of continuous recording the baseline slightly increased to 505 ± 1 pA which corresponded to a variation of 1.6 %. This result shows that, nanobridge configuration, was not affected by evaporation which would result in much larger fluctuations and instability in the signal due to salt crystal formation at the tip of the nanopipette. (b). I-V characterization before and after use as show minimal observable change in the ionic current.

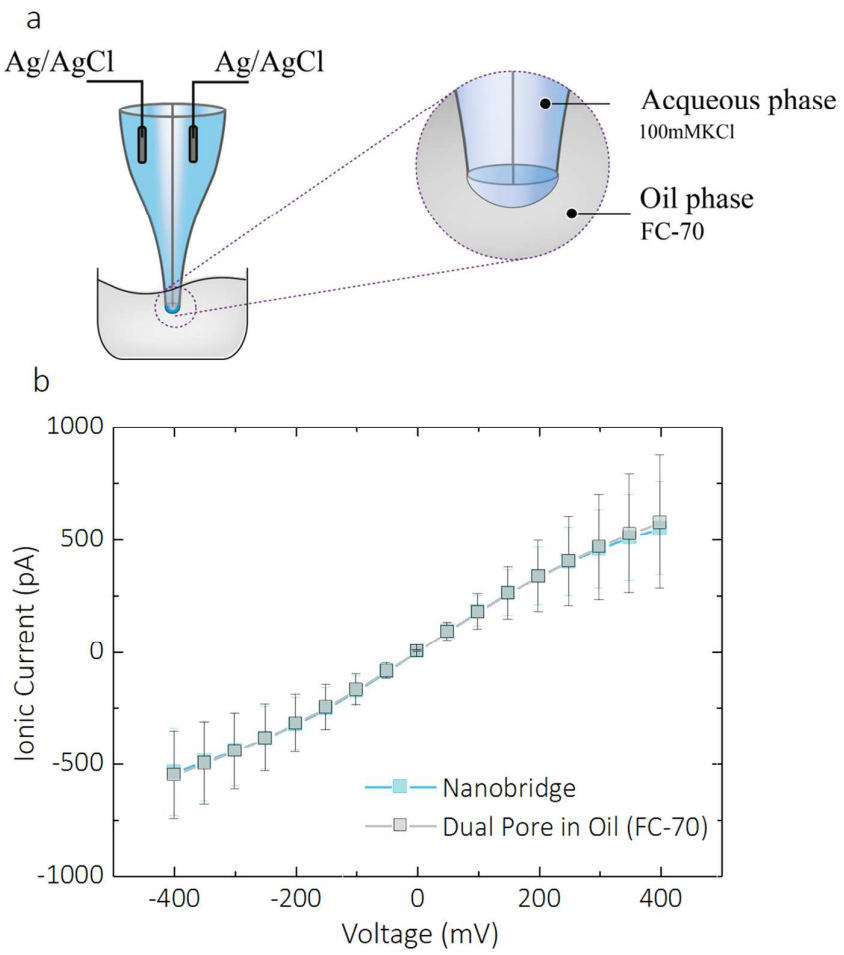

Figure S5. Characterization of droplet stability using the nanobridge configuration submersed in oil. In addition to long term stability recordings, Supplementary Figure 4, nanobridge control IV were measured for nanobridge configuration in air and immersed in an immiscible fluorinated oil (FC-70, Sigma Aldrich), where electrolyte evaporation is unlikely to occur (a) Schematic of the experiments (b) I-V characterization for both the nanobridge configuration in air and the nanobridge immersed in oil showing minimal deviation and indicating that under the experimental conditions used, electrolyte is efficiently replenished at the nanopipette tip and evaporation has negligible effect on the open-pore current. All experiments were performed in 100 mM KCl 10 mM Tris 1 mM EDTA at pH 8.0 and recorded using a Multiclamp 700B (Molecular Devices, USA).

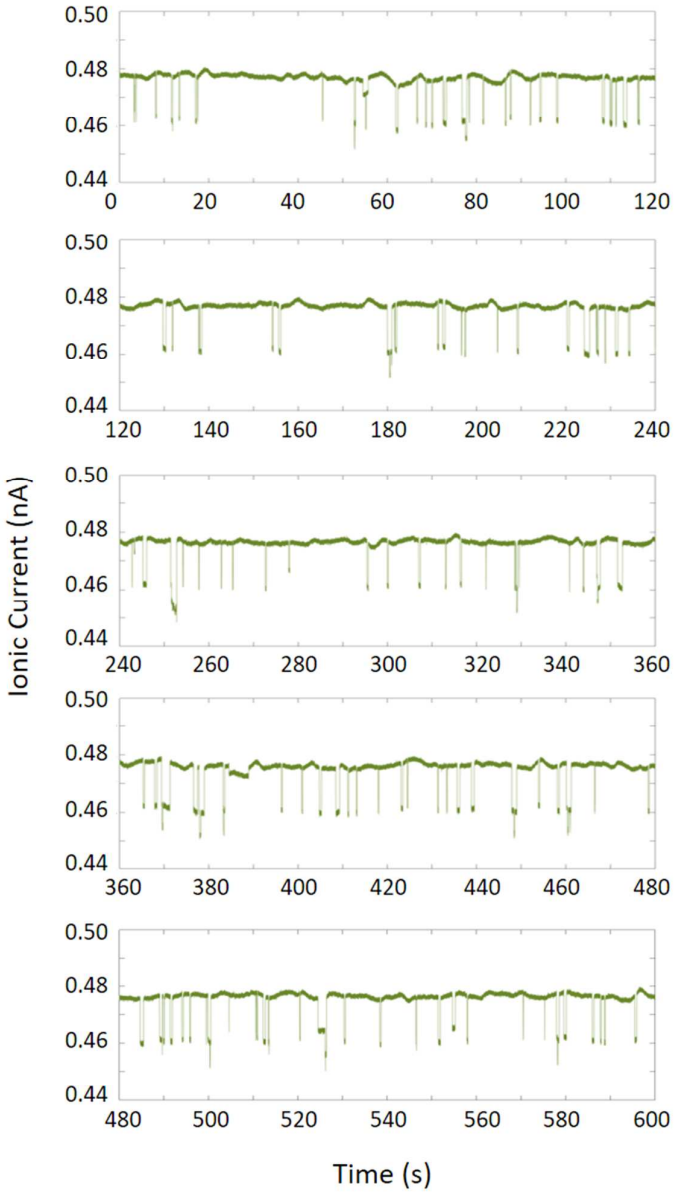

Figure S6. dsDNA translocation stability over time in nanobridge configuration. Representative trace showing stable average baseline current and consistent current blockade signatures over 10 minutes**.** Both barrels of the nanopipette were filled with 200 pM 10 kbp DNA in 100 mM KCl and current-time traces were recorded at 225 mV and resampled at 1 kHz for visualisation. Five consecutive recordings of two minutes each are plotted and, as it can be seen, not only the baseline but also the peak amplitude of individual events was very similar over the time.

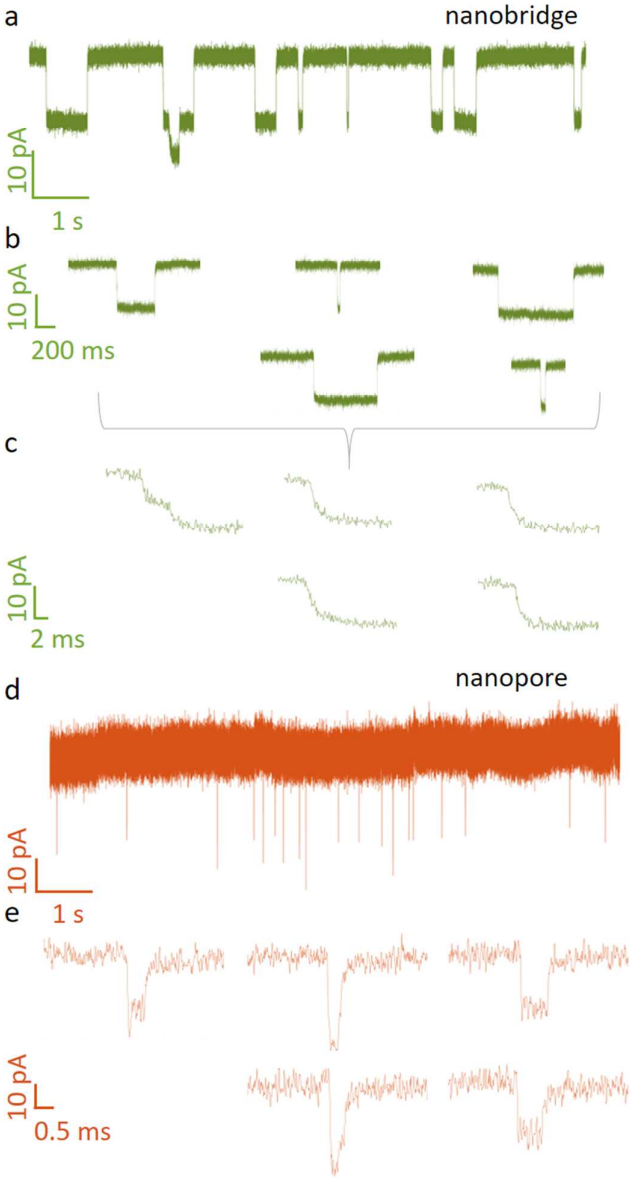

Figure S7. Comparison between translocations performed in the nanobridge and nanopore (conventional) configurations. Experiments were performed using 200 pM 10 kbp DNA and performed in 100 mM KCl, 10 mM Tris 1 mM EDTA (pH 8.0) with an applied bias of 200 mV. (a) Current-time traces and (b-c) zoomed in translocation events using the nanobridge (resampled at 10 kHz). (d) Current-time traces and (e) zoomed in translocation events using the conventional configuration (filtered at 10 kHz). Importantly within the nanobridge configuration the slow decay followed by the current blockade are clearly visible, whereas in the conventional configuration translocations have much more abrupt transitions.

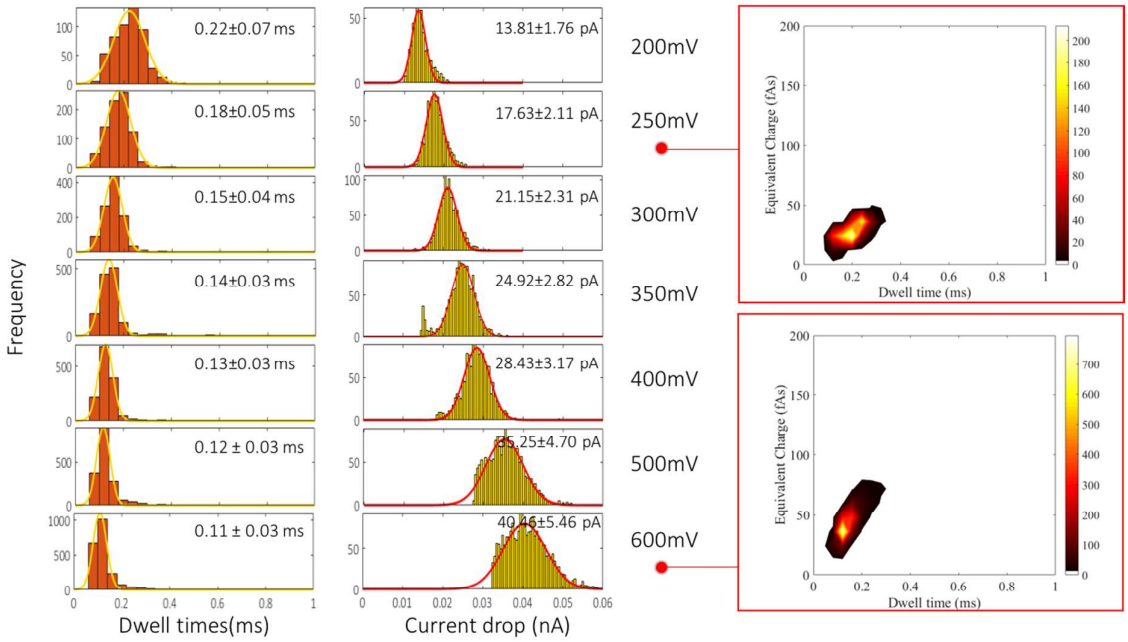

Figure S8. Dwell time and current blockade dependence on voltage for 400 pM 5 kbp DNA in nanopore (conventional) configuration. All experiments were performed in 100 mM KCl, 10 mM Tris, 1 mM EDTA at pH 8.0. translocations were consistent with what has been reported in the literature. For example, DNA translocation decreased with the voltage applied from 0.22 ± 0.07 ms at 200 mV to 0.11 ± 0.03 ms at 600 mV while the peak current blockade followed the opposite trend going from 13.81 ± 1.76 pA to 40.46 ± 5.46 pA.

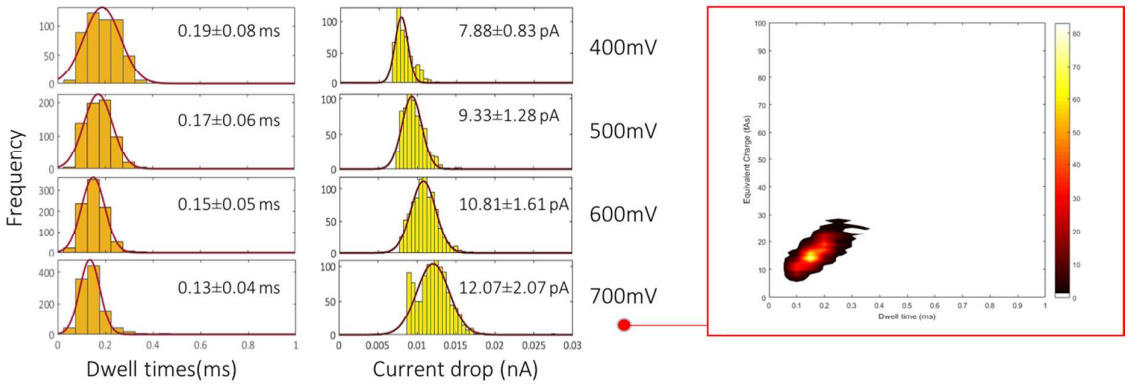

Figure S9. Dwell time and current blockade dependence on voltage for 400 pM 5 kpb DNA using the dual nanopore configuration in electrolyte bath. All experiments were performed in 100 mM KCl, 10 mM Tris, 1 mM EDTA at pH 8.0. This configuration can be assumed to be similar to the conventional configuration with exception that in this system there is extra resistance due to the introduction of the second nanopore resulting in lower current blockades. Translocation times were similar to the conventional configuration (e.g. 0.19 ± 0.08 ms at 400 mV).

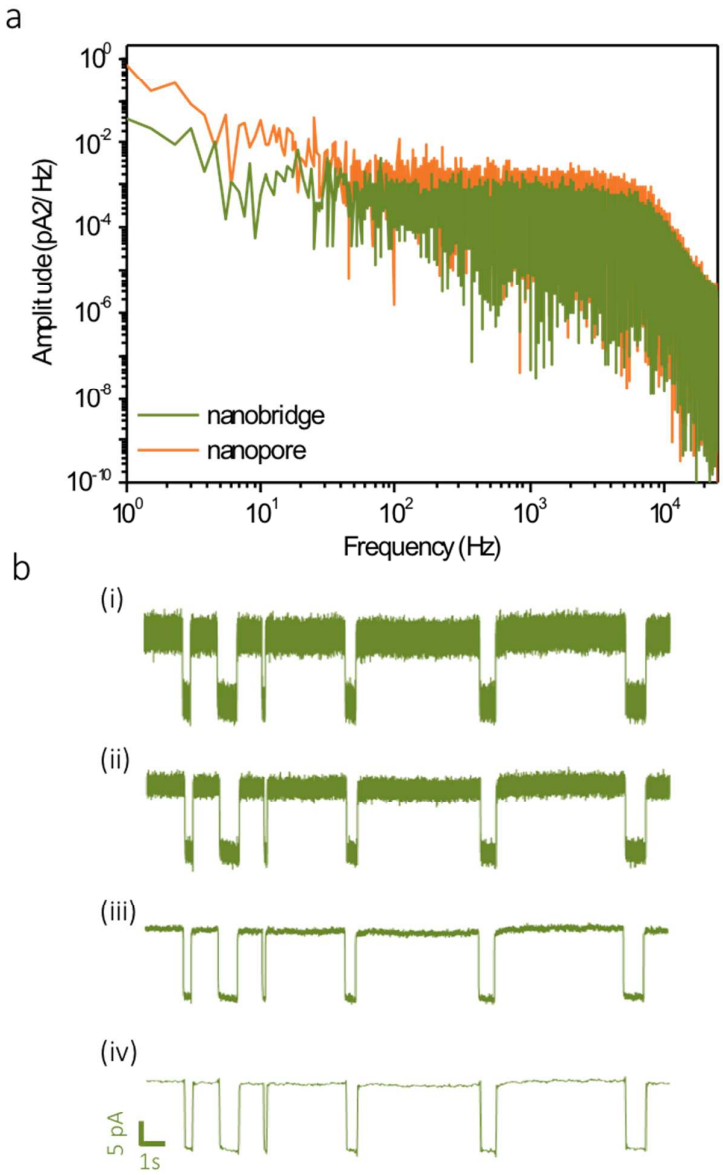

Figure S10. Power spectral density and resampling analysis. (a) Power spectral densities of nanopipettes in conventional and nanobridge configuration, under a negative 300 mV applied bias. Both signals were filtered at 5 kHz. The nanobridge showed superior performances in the low-medium frequency regime. However, due to long translocation times, high bandwidth recordings were not required. Therefore, the current-time trace can either be recorded at lower bandwidth or resampled accordingly to improve the SNR. This significant advantage is at no cost to the information being obtained. (b) As an example, current-time traces of 10 kbp DNA in 100 mM KCl are shown and resampled at frequencies of (i) 100 kHz, (ii) 10 kHz, (iii) 1 kHz and, (iv) 100 Hz. As expected it can be clearly seen that the SNR improves dramatically.

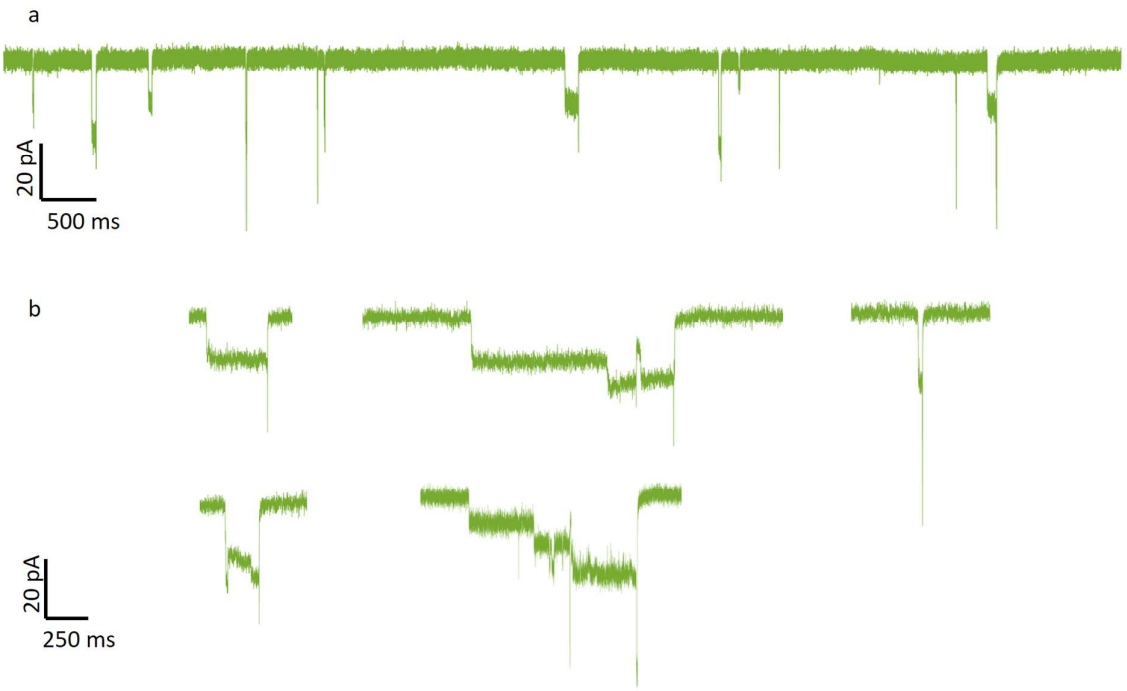

Figure S11. Examples of multistep behaviour for the translocation of M13 ssDNA using the nanobridge configuration. Experiments were performed at a DNA concentration of 100 pM in a buffer consisting of 100 mM KCl, 10 mM Tris, 1mM EDTA (pH 8.0) at an applied bias of 400 mV. Unlike dsDNA multistep behaviour was common and likely attributed to the crowding and tighter packing of the DNA in the nanobridge. This is evident in the (a) ionic current-time trace (b) zoom in of representative translocation events. This is consistent with the fraction of multistep events increasing as voltage is increased, see Figure 6 in the main text.

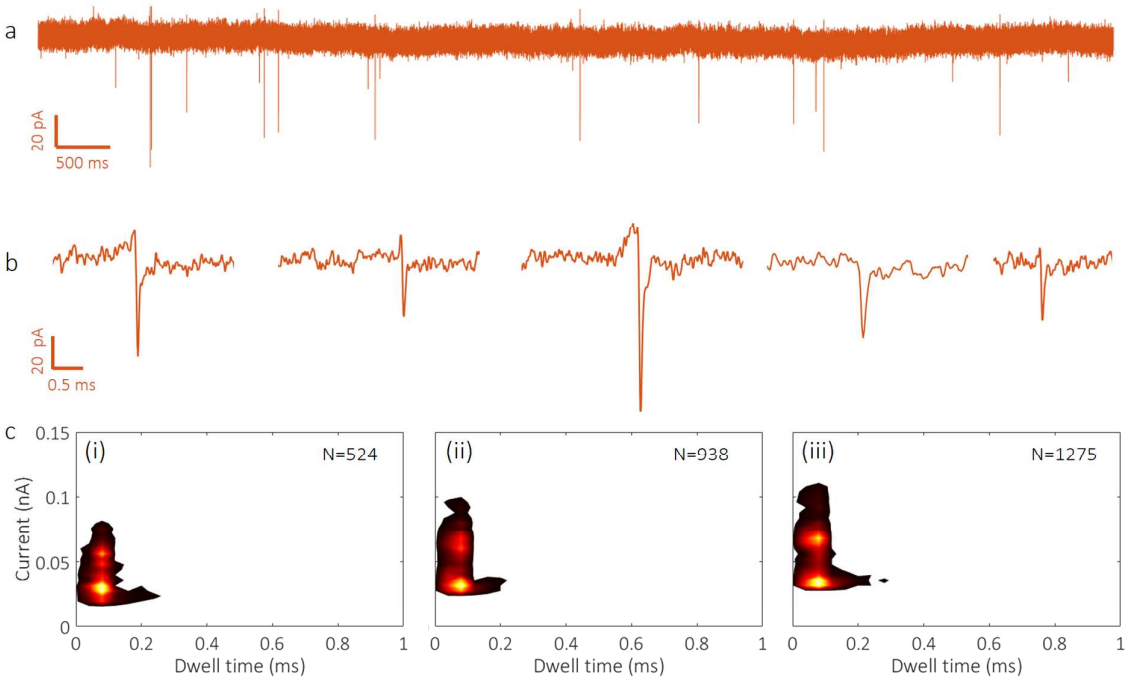

Figure S12. Current-time trace for M13 ssDNA performed using the conventional configuration. Experiments were performed at a DNA concentration of 100 pM in a buffer consisting of 100 mM KCl, 10 mM Tris, 1 mM EDTA (pH 8.0) at an applied bias of 400 mV. (a) Current – time trace along with representative (b) zoomed in events are shown. In contrast with the nanobridge events threaded through the pore at high velocity with sub-ms dwell times. The biphasic behaviour was in good agreement with what has been previously reporter for the same molecule in similar ionic strength within the literature. (c) Surface density plots of ssDNA at i) 300 mV ii) 400 mV and iii) 500 mV.